Science Advances
AAAS

advances.sciencemag.org/cgi/content/full/4/8/eaat8978/DC1

Supplementary Materials for

Robust optical polarization of nuclear spin baths using Hamiltonian engineering of nitrogen-vacancy center quantum dynamics

Ilai Schwartz*, Jochen Scheuer, Benedikt Tratzmiller, Samuel Müller, Qiong Chen*, Ish Dhand, Zhen-Yu Wang, Christoph Müller, Boris Naydenov, Fedor Jelezko, Martin B. Plenio*

*Corresponding author. Email: qiong.chen@uni-ulm.de (Q.C.); ilai.schwartz@uni-ulm.de (I.S.); martin.plenio@uni-ulm.de (M.B.P.)

Published 31 August 2018, *Sci. Adv.* **4**, eaat8978 (2018)
DOI: 10.1126/sciadv.aat8978

This PDF file includes:

Supplementary Text
Section S1. Hamiltonian of the system
Section S2. Effective Hamiltonian of PulsePol
Section S3. Error robustness
Section S4. Finite pulses
Section S5. Composite pulses
Section S6. Effect of phase errors
Section S7. Hamiltonian with NV centers in nanodiamonds
Section S8. Depolarization behavior
Section S9. Simulation parameters for shallow NV centers
Fig. S1. MW pulse sequence for pulsed polarization transfer.
Fig. S2. Error resistance of PulsePol by using composite pulses.
Fig. S3. Effect of phase errors.
Fig. S4. Error resistance of PulsePol versus the resonance shift.
Fig. S5. Comparison between simulation results and experimental data of polarization buildup and depolarization.

Supplementary Information

Section S1. Hamiltonian of the system

We consider a system of a single electron spin $\vec{S}$ ($S = \frac{1}{2}$) coupled to N nuclear spins $\vec{I}^{(n)}$ (spin-1/2). The System is described by the Hamiltonian

$$H = \omega_S S_z + \sum_{n=1}^{N} \omega_I I_z^{(n)} + \sum_{n=1}^{N} \vec{S}\mathcal{A}\vec{I}^{(n)} + 2\Omega(t) S_x \cos(\omega_{MW} t + \varphi) \tag{1}$$

where $\omega_S(\omega_I)$ denotes the electron (nuclear) Larmor frequency, $\mathcal{A}$ the hyperfine coupling tensor describing the interaction between electron and nuclear spins resulting from the magnetic dipole-dipole coupling, ω_{MW} the microwave frequency, φ the microwave phase, and the Rabi frequency $\Omega(t)$ has the value Ω_0 when the microwave is on, and 0 otherwise.
In a rotating frame with respect to $\omega_S S_z$ and after applying the secular approximation, the Hamiltonian is

$$H_{\text{int}} = \Delta S_z + \sum_{n=1}^{N} \omega_I I_z^{(n)} + \sum_{n=1}^{N} S_z \vec{\mathcal{A}}\vec{I}^{(n)} + \Omega(t)(S_x \cos\varphi + S_y \sin\varphi) \tag{2}$$

with $\Delta = \omega_S - \omega_{MW}$ denoting the detuning between the MW and electron Larmor frequency. In a nuclear spin basis such that $A_y = 0$ we obtain the basic Hamiltonian:

$$H_{\text{int}} = \Delta S_z + \sum_{n=1}^{N} \omega_I I_z^{(n)} + \sum_{n=1}^{N} S_z \left(A_x I_x^{(n)} + A_z I_z^{(n)} \right) + \Omega(t)(S_x \cos\varphi + S_y \sin\varphi) \tag{3}$$

According to this Hamiltonian, the free evolution operator for a time τ is

$$\begin{aligned} U_{\text{free}}(\tau) &= \exp\left(-i\tau \left(\Delta S_z + \sum_{n=1}^{N} \omega_I I_z^{(n)} + \sum_{n=1}^{N} S_z \left(A_x I_x^{(n)} + A_z I_z^{(n)} \right) \right) \right) \\ &= \exp\left(-i\tau \left(\sum_{n=1}^{N} \omega_I I_z^{(n)} + \sum_{n=1}^{N} S_z \left(A_x I_x^{(n)} + A_z I_z^{(n)} \right) \right) \right) \exp\left(-i\tau \Delta S_z \right) \end{aligned} \tag{4}$$

where the last equality holds as the ΔS_z term commutes with the other terms in the exponent.
The pulses have an additional Rabi term and are described by

$$U_{\phi,\pm\text{X}/\pm\text{Y}} = \exp\left(-i\frac{\phi}{\Omega_0} \left(\Delta S_z + \sum_{n=1}^{N} \omega_I I_z^{(n)} + \sum_{n=1}^{N} S_z \left(A_x I_x^{(n)} + A_z I_z^{(n)} \pm \Omega_0 S_{\text{X/Y}} \right) \right) \right) \tag{5}$$

As it is difficult to understand the dynamics from this description, the next section uses a model with only one nuclear spin to derive an effective Hamiltonian.

Section S2. Effective Hamiltonian of PulsePol

The PulsePol sequence as shown in the text is given by

$$\left[\left(\frac{\pi}{2}\right)_Y \overset{\tau/4}{\text{——}} (\pi)_X \overset{\tau/4}{\text{——}} \left(\frac{\pi}{2}\right)_Y \left(\frac{\pi}{2}\right)_{-X} \overset{\tau/4}{\text{——}} (\pi)_Y \overset{\tau/4}{\text{——}} \left(\frac{\pi}{2}\right)_{-X} \right]^{2N} \tag{6}$$

where $(\phi)_{X,\pm Y}$ denote pulses around the X-/Y-axis with duration $t' = \phi/\Omega$ and phase $\varphi = 0, \pm\pi/2$ and $\overset{\tau/4}{\text{——}}$ denotes a free evolution for a time $\tau/4$, which depends on the nuclear Larmor frequency. The basic sequence block is repeated $2N$ times, where N is a positive integer.

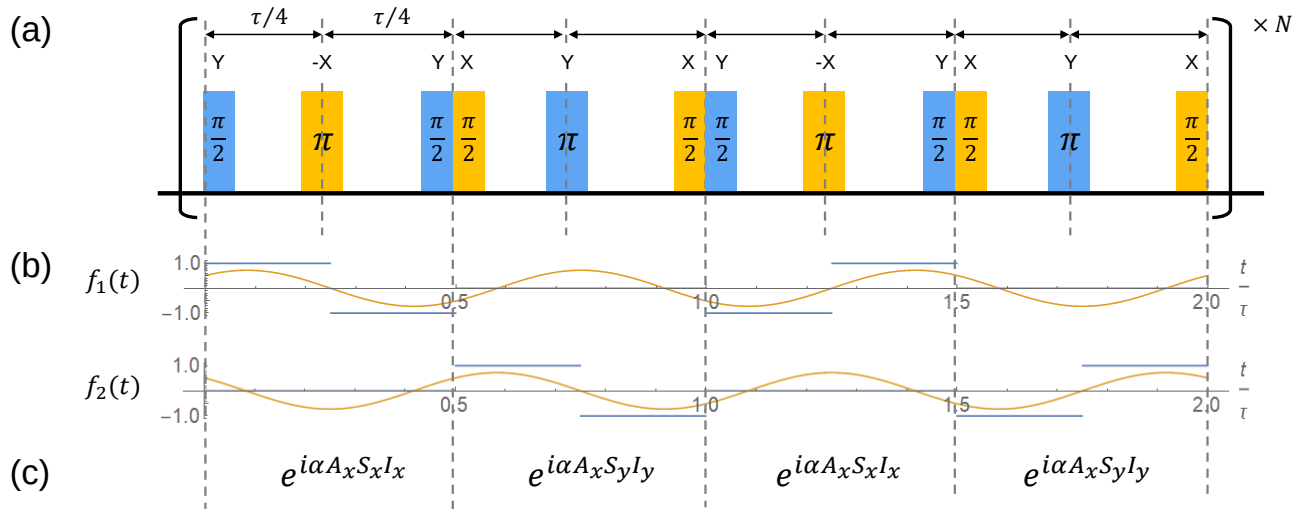

Fig. S1. MW pulse sequence for pulsed polarization transfer. (a) Schematics of the MW pulse sequence on the electron spin for pulsed polarisation transfer to nuclear spins. Blue bars denote Y pulses and orange ones X or -X pulses. The sequence alternates between four sections. (b) The values of the modulation functions for the sections are $f_1(t) \sim \cos(3\pi t/\tau - \pi/4)$ and $f_2(t) \sim -\sin(3\pi t/\tau - \pi/4)$ for S_x and S_y (blue), and their dominant Fourier component (orange) (c) The pulse sequence produces 4 distinct sections, each with an effective Hamiltonian in the rotating frame. The combination of a basis change for the electron spin in each section with the $\pi/2$ phase shift in the modulation function leads to the effective average Hamiltonian $S_x I_x + S_y I_y = 1/2(S_+ I_- + S_- I_+)$ which produces the polarisation transfer between electron spin and nuclei.

Here we express the spin operators in terms of the Pauli matrices σ_i ($i \in \{x, y, z\}$): $S_i = \frac{1}{2}\sigma_i$. According the PulsePol sequence in Eq. (6), by using $U_{\frac{\pi}{2},\mathrm{X}} \begin{pmatrix}\sigma_x\\ \sigma_y\\ \sigma_z\end{pmatrix} U_{\frac{\pi}{2},\text{-X}} = \begin{pmatrix}\sigma_x\\ \sigma_z\\ -\sigma_y\end{pmatrix}$ and $U_{\frac{\pi}{2},\mathrm{Y}} \begin{pmatrix}\sigma_x\\ \sigma_y\\ \sigma_z\end{pmatrix} U_{\frac{\pi}{2},\text{-Y}} = \begin{pmatrix}-\sigma_z\\ \sigma_y\\ \sigma_x\end{pmatrix}$, one can rewrite the evolution as

$$U_{\text{cycle}} = U_{\frac{\tau}{4},\text{-Y}} U_{\frac{\tau}{4},\mathrm{Y}} U_{\frac{\tau}{4},\text{-X}} U_{\frac{\tau}{4},\mathrm{X}} U_{\frac{\tau}{4},\mathrm{Y}} U_{\frac{\tau}{4},\text{-Y}} U_{\frac{\tau}{4},\mathrm{X}} U_{\frac{\tau}{4},\text{-X}} \tag{7}$$

where

$$U_{\tau,\pm\mathrm{X}/\pm\mathrm{Y}} = \exp\left(-i \sum_{n=1}^{N} \tau \left(\omega_I I_z^{(n)} \pm S_{x/y}(A_x I_x^{(n)} + A_z I_z^{(n)})\right)\right) \tag{8}$$

This means the evolution can be expressed with an effective Hamiltonian

$$H_{\text{eff}}^{(1)} = \sum_{n=1}^{N} \omega_I I_z^{(n)} + (-f_1(t) S_x - f_2(t) S_y)(A_x I_x^{(n)} + A_z I_z^{(n)}) \tag{9}$$

The functions $f_{1/2}$ and how they emerge from the sequence are shown in figure S1. They can be expressed as Fourier series

$$\begin{aligned} f_1(t + k \cdot 2\tau) &= \begin{cases} 1, & \text{for } 0\tau \leqslant t \leqslant \tau/4,\ 5\tau/4 \leqslant t \leqslant 3\tau/2 \\ -1, & \text{for } \tau/4 \leqslant t \leqslant \tau/2,\ \tau \leqslant t \leqslant 5\tau/4 \\ 0, & \text{otherwise} \end{cases} \\ &= \sum_{n=0}^{\infty} a_n^{(1)} \cos\frac{\pi n t}{\tau} + b_n^{(1)} \sin\frac{\pi n t}{\tau} \end{aligned} \tag{10}$$

and

$$f_2(t + k \cdot 2\tau) = f_1\left(t - \frac{\tau}{2}\right) = \sum_{n=0}^{\infty} a_n^{(2)} \cos\frac{\pi n t}{\tau} + b_n^{(2)} \sin\frac{\pi n t}{\tau} \tag{11}$$

The Fourier coefficients can be calculated as

$$a_n^{(1)} = \frac{2}{2\tau}\int_0^{8\tau} f_1(t)\cos\frac{\pi n t}{\tau} = \frac{1}{\pi n}\frac{1-(-1)^n}{2}\left[4\sin\frac{\pi n}{4} - 2\sin\frac{\pi n}{2}\right] \tag{12}$$

This expression equals 0 for every even value of n, the same holds for

$$b_n^{(1)} = \frac{2}{2\tau}\int_0^{8\tau} f_1(t)\sin\frac{\pi n t}{\tau} = \frac{1}{\pi n}\frac{1-(-1)^n}{2}\left[-4\sin\frac{\pi n}{4} + 2\right] \tag{13}$$

Due to the shift in the modulation functions 11 we get similar coefficients for f_2, $|a_n^{(2)}| = |b_n^{(1)}|$ and $|b_n^{(2)}| = |a_n^{(1)}|$. Notice that $a_1^{(1)} = -b_1^{(1)} = \frac{2}{\pi}\left(\sqrt{2}-1\right)$ and $a_3^{(1)} = b_3^{(1)} = \frac{2}{3\pi}\left(\sqrt{2}+1\right)$ result in $|a_3^{(1)}| \approx 1.94\,|a_1^{(1)}|$, which is the reason we choose the third order, namely $a_3^{(1)}$ and $b_3^{(1)}$. The related Fourier terms corresponding to $a_3^{(1)}$ and $b_3^{(1)}$ are plotted in the upper figure S1. This is achieved by choosing

$$\tau = 3\frac{\pi}{\omega_I} \tag{14}$$

In a rotating frame with respect to $\omega_I I_z$, discarding all fast-rotating terms, we get

$$\begin{aligned} H_{avg} &= -\sum_{n=1}^{N}\frac{A_x}{2}a_3^{(1)}\left(S_x I_x^{(n)} + S_y I_x^{(n)} - S_x I_y^{(n)} + S_y I_y^{(n)}\right) \\ &= -\sum_{n=1}^{N}\frac{A_x}{4}\alpha\left(\tilde{S}_- I_+^{(n)} + \tilde{S}_+ I_-^{(n)}\right) \end{aligned} \tag{15}$$

with $\alpha = \sqrt{a_3^{(1)} + b_3^{(1)}} = \frac{2}{3\pi}(2+\sqrt{2})$. The basis change resulting from $\tilde{S}_x = (S_x + S_y)\sqrt{2}$ and $\tilde{S}_y = (-S_x + S_y)\sqrt{2}$ does not affect the polarisation dynamics as only the x-y-plane is rotated and the z-axis remains.

Section S3. Error robustness

As a robust polarisation sequence PulsePol should meet the following criteria (i)-(iii) from the main text:
(i) It produces both S_x and S_y terms in the effective Hamiltonian with the modulation functions $f_1(t)$, $f_2(t)$, preferably by producing the phase change $f_2(t) = f_1(t + \pi/2)$.
(ii) The detuning errors accumulated during the free evolution need to be cancelled and preferably also decoupled from unwanted noise and fluctuations.
(iii) as pulses are not perfect, i.e. of a finite length and with detuning and Rabi frequency errors, the polarisation sequence should cancel such errors at least to the first order.
As criterion (i) is fulfilled as already shown in the previous section, we present the detailed proofs of the other criteria (ii) and (iii) as follows.
Criterion (ii), the cancellation of detuning errors accumulated during the free evolution, follows from the anti-commutation relation of Pauli matrices $[\sigma_{x/y}, \sigma_z]_+ = 0$. This relation can be used to derive the property $\exp(-i\tau\Delta S_z)\, S_{x/y} = S_{x/y}\exp(+i\tau\Delta S_z)$. As the ΔS_z term commutes with the rest of the free evolution, one can see the cancellation of the detuning errors accumulated during the free evolution around every perfect π pulse in the evolution operator with the help of (4)

$$U_{\text{free}}(\tau)U_{\pi,\text{X/Y}}U_{\text{free}}(\tau) = U_{\text{free}}(\tau)2S_{x/y}U_{\text{free}}(\tau) \tag{16}$$

$$= e^{-i\tau(\omega_I + S_z A_x I_x)}e^{-i\tau\Delta S_z}2S_{x/y}e^{-i\tau\Delta S_z}e^{-i\tau(\omega_I + S_z A_x I_x)} \tag{17}$$

$$= U_{\text{free},\Delta=0}(\tau)U_{\pi,\text{X/Y}}U_{\text{free},\Delta=0}(\tau). \tag{18}$$

The cancellation happens in every part of the sequence, leading to complete cancellation of detuning errors for perfect pulses. This means that improving the pulses also corrects errors accumulated during the free evolution.

For criterion (iii), the cancellation of pulse errors to 1st order, is fulfilled. Including a Rabi frequency error $\delta\Omega = \Omega_0 - \tilde{\Omega}_0$, the pulses with errors take the form

$$U_{\theta,\pm X/Y} = \exp\left(-i\frac{\theta}{\Omega}\left(\pm\tilde{\Omega}S_{x/y} + \Delta S_z\right)\right) \tag{19}$$

Introducing the definitions $\frac{\Delta}{\Omega} \equiv \epsilon k_1$ and $\frac{\Omega}{\tilde{\Omega}} = 1 - \frac{\delta\Omega}{\Omega} \equiv 1 + \epsilon k_2$, it is straightforward to show that in the evolution operator of one sequence block, neglecting the nuclear spins, the detuning and Rabi errors have an overall effect of

$$U_{\pi/2,-X}U_{\pi,Y}U_{\pi/2,-X}U_{\pi/2,Y}U_{\pi,X}U_{\pi/2,Y}U_{\pi/2,-X}U_{\pi,Y}U_{\pi/2,-X}U_{\pi/2,Y}U_{\pi,X}U_{\pi/2,Y} \tag{20}$$

$$= -(\mathbb{1} + \epsilon^2 k_1^2(-2i\sigma_z) + \epsilon^3 k_1^2 k_2 2\pi i\sigma_z) + O(\epsilon^4) \tag{21}$$

This means in the pulses Rabi errors are cancelled up to second order, detuning errors in first order. Note that the second order in detuning errors is a z-rotation and can therefore be compensated with a tau-shift for a specific detuning value, as shown for phase errors later. This completes the proof that the PulsePol sequence fulfills all of the desired properties. Notice that the PulsePol sequence is not the only option but the best sequence found. It can be derived as the simplest sequence fulfilling the above criteria (i)-(iii).
There are other possible sequences fulfilling the above properties, for example the PolXY sequence

$$\begin{aligned}\left(\frac{\pi}{2}\right)_Y \Bigg[&\overset{\tau/2}{\text{---}} (\pi)_X \overset{\tau}{\text{---}} (\pi)_Y \overset{\tau}{\text{---}} (\pi)_X \overset{\tau}{\text{---}} (\pi)_Y \overset{\tau/2}{\text{---}} \\ &\left(\frac{\pi}{2}\right)_X \overset{\tau}{\text{---}} (\pi)_Y \overset{\tau}{\text{---}} (\pi)_X \overset{\tau}{\text{---}} (\pi)_Y \overset{\tau}{\text{---}} \left(\frac{\pi}{2}\right)_X \Bigg]^N \left(\frac{\pi}{2}\right)_{-Y}\end{aligned} \tag{22}$$

with a resonance for $\tau = n\pi/\omega_L$, but PulsePol has the best properties concerning error stability. Furthermore PolXY and other sequences showed an undesired depolarisation behaviour for detuning values close to the Rabi frequency, which is significantly reduced for PolsePol as shown in section S8.
A sequence which has almost identical behaviour to PulsePol is

$$\left[\left(\frac{\pi}{2}\right)_Y \overset{\tau/4}{\text{---}} (\pi)_Y \overset{\tau/4}{\text{---}} \left(\frac{\pi}{2}\right)_{-Y} \left(\frac{\pi}{2}\right)_X \overset{\tau/4}{\text{---}} (\pi)_X \overset{\tau/4}{\text{---}} \left(\frac{\pi}{2}\right)_{-X}\right]^{2N} \tag{23}$$

Combining this with the actual PulsePol sequence leads to

$$\begin{aligned}\Bigg[\Bigg[\left(\frac{\pi}{2}\right)_Y &\overset{\tau/4}{\text{---}} (\pi)_X \overset{\tau/4}{\text{---}} \left(\frac{\pi}{2}\right)_Y \left(\frac{\pi}{2}\right)_{-X} \overset{\tau/4}{\text{---}} (\pi)_Y \overset{\tau/4}{\text{---}} \left(\frac{\pi}{2}\right)_{-X}\Bigg]^2 \\ \Bigg[\left(\frac{\pi}{2}\right)_Y &\overset{\tau/4}{\text{---}} (\pi)_Y \overset{\tau/4}{\text{---}} \left(\frac{\pi}{2}\right)_{-Y} \left(\frac{\pi}{2}\right)_X \overset{\tau/4}{\text{---}} (\pi)_X \overset{\tau/4}{\text{---}} \left(\frac{\pi}{2}\right)_{-X}\Bigg]^2\Bigg]^N\end{aligned} \tag{24}$$

which behaves as PulsePol, but here no oscillations for changing detuning values are present.
The latter two sequences and PulsePol itself can be derived with the following steps:

1. Criterion (i) suggests that the modulation functions of such a sequence of length 2τ consists of four different parts, $f_1(t) = 0$ in the second and fourth part represents a specific basis choice and $f_2(t) = f_1(t - \tau/2)$ represents the correct phase difference.
2. As detuning errors need to be cancelled according to criterion (ii), a relation similar to (16) needs to be fulfilled, i.e. the sequence must consist of blocks like $\overset{t}{\text{---}} (\pi)_\Phi \overset{t}{\text{---}}$. This, combined with 1., immediately leads to the modulation functions in figure S1(b).
3. The basis changes, criterion (i), require $\pi/2$-pulses before and after these blocks, the error cancellation (iii) determines the form to be $\left(\frac{\pi}{2}\right)_{\pm Y} \overset{t}{\text{---}} (\pi)_Y \overset{t}{\text{---}} \left(\frac{\pi}{2}\right)_{\mp Y}$ or $\left(\frac{\pi}{2}\right)_{\pm X} \overset{t}{\text{---}} (\pi)_Y \overset{t}{\text{---}} \left(\frac{\pi}{2}\right)_{\pm X}$ up to rotations and basis changes.

This leads to the PulsePol sequence (6) and other options like (23), (24).

Section S4. Finite pulses

In section S2 pulses were assumed to be perfect. With a finite Rabi frequency they also take a finite time, during which all parts of the system evolve, increasing the total time needed for every sequence block. In order to compensate that, the evolution times need to be reduced. As a block contains free evolutions lasting 2τ, eight $\pi/2$-pulses and four π-pulses, the free evolution time is

$$\tau = \frac{\pi}{\omega_I} \times n - \frac{4}{2} t_\pi - \frac{8}{2} t_{\pi/2} \tag{25}$$

where t_π and $t_{\pi/2}$ denote the time needed for π- and $\pi/2$-pulses. In case of simple pulses, the expression reduces to

$$\tau = \frac{\pi}{\omega_I} \times n - \frac{4}{2}\frac{\pi}{\Omega_0} - \frac{8}{2}\frac{\pi}{2\Omega_0} = \frac{\pi}{\omega_I} \times n - 4\frac{\pi}{\Omega_0} \tag{26}$$

In case of different pulses like in section S5, the correction term changes with the pulse times. In all cases it is important that the pulses do not reduce the free evolution time by a significant amount, simulations show that the pulse time should be less than 20% of the free evolution time. To reach this regime even for long pulses, the parameter n can be increased as described in the previous section.

Section S5. Composite pulses

The stability with respect to both detuning and Rabi frequency errors can be increased with composite pulses, which are designed to correct those errors within the pulses. As our main goal is to get reliable polarisation transfer for a wide range of detunings, we focus on the correction of detuning errors over Rabi frequency errors here.
In the numerical simulations we used different sequences described in (*18*). Best results were achieved with the pulses

$$90 = \overline{16}\ \ 300\ \ \overline{266}\ \ 54\ \ \overline{266}\ \ 300\ \ \overline{16} \tag{27}$$

for $\pi/2$ pulses and

$$180 = 325\ \ \overline{263}\ \ 56\ \ \overline{263}\ \ 325 \tag{28}$$

for π pulses.
The composite pulses mentioned above rotate around angles of $1218/180 \times \pi$ and $1232/180 \times \pi$, respectively, which means according to equation (25) that for PulsePol

$$\tau = \frac{\pi}{\omega_I} \times l - \left(2\frac{1232}{180} + 4\frac{1218}{180}\right)\frac{\pi}{\Omega_0} \tag{29}$$

The resulting error robustness is shown in figure S2 The composite pulses allow for significantly larger detuning (For $\Omega = 50$ MHz more than ± 40 MHz) than in case of shorter pulses considered. The results aren't improved by choosing even longer composite pulses, because the pulse duration should not take a large fraction of the free evolution time.

Section S6. Effect of phase errors

In figure S3 one can see the analytically calculated (first order) and the simulated dependence of the shift in resonance depending on a phase error α: In the PulsePol sequence, we assume every $\pi/2$ pulse that follows another pulse without a free evolution in between has a shifted phase

$$\left[\left(\frac{\pi}{2}\right)_{\overline{Y}} \overset{\tau/4}{\text{——}} (\pi)_X \overset{\tau/4}{\text{——}} \left(\frac{\pi}{2}\right)_Y \left(\frac{\pi}{2}\right)_{\overline{-X}} \overset{\tau/4}{\text{——}} (\pi)_Y \overset{\tau/4}{\text{——}} \left(\frac{\pi}{2}\right)_{-X}\right]^{2N} \tag{30}$$

where $\overline{Y} = Y\cos\alpha - X\sin\alpha$ and $\overline{-X} = -X\cos\alpha + Y\sin\alpha$.

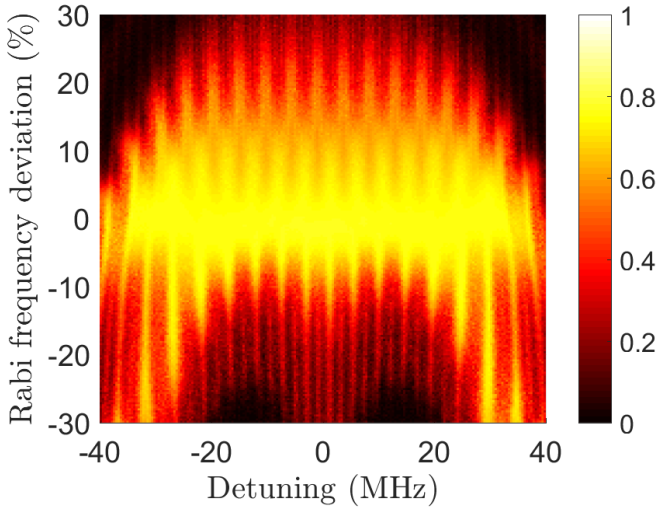

Fig. S2. Error resistance of PulsePol by using composite pulses. Error-resistance (polarisation transfer vs. Δ and $\delta\Omega/\Omega_0$) for PulsePol with composite pulses, parameters as in Fig. 2c in the main text: $\omega_I = 2$ MHz, $A_x = 0.03$ MHz and $\Omega_0 = 50$ MHz. Here the $l = 5$ resonance was used.

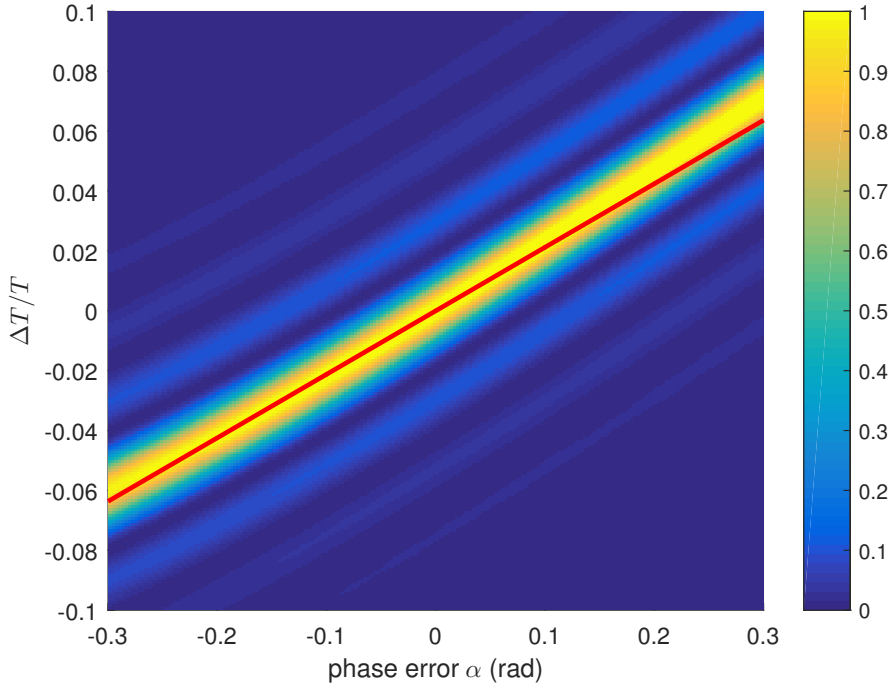

Fig. S3. Effect of phase errors. Simulated and calculated (red line, first order) dependence of the resonance shift on the error α. A high function value (yellow) indicated that the protocol works well for the corresponding parameters.

This description has the same effect as standard phase errors, we choose it as in the experiment the shift in resonance condition originates from this effect. For $\tau = 0$ in first order of α, the overall effect of this on the NV is described by

$$(U_{\pi/2,-X}U_{\pi,Y}U_{\pi/2,\overline{-X}}U_{\pi/2,Y}U_{\pi,X}U_{\pi/2,\overline{Y}})^2 \tag{31}$$

$$= \left(U_{\pi/2,-X}U_{\pi,Y}\left(U_{\pi/2,-X} + \frac{\alpha}{\sqrt{2}}U_{\pi,Y}\right)U_{\pi/2,Y}U_{\pi,X}\left(U_{\pi/2,Y} + \frac{\alpha}{\sqrt{2}}U_{\pi,-X}\right)\right)^2 + O(\alpha)^2 \tag{32}$$

$$= \exp\left(-4i\alpha S_z\right) + O(\alpha)^2 \tag{33}$$

This means the NV basis is rotated by -2α in the x-y-plane during the time 2τ. After a rotation of $-\pi$, the

modulation functions are inverted. This corresponds to a shift of half a period in the modulation functions, which corresponds to a time

$$\Delta T = \frac{1}{2n} 2\tau \tag{34}$$

where n is the (odd) resonance condition chosen.
Assuming the sequence needs M cycles for a π shift, we can determine the relation between the resonance shift and the phase error

$$\frac{\Delta T/T}{\alpha} = \frac{\tau/n \times 1/(2\tau M)}{\pi/(4M)} = \frac{2}{\pi n} \tag{35}$$

The corresponding line is plotted in figure S3 for $n = 3$. Especially around $\alpha = 0$, where higher orders are negligible, it fits the simulation very well.
Note that this is a continuous process of shifting the modulation functions and therefore has a direction as the modulation functions are shifted by $\pi/2$. For $n = 5$ the shift is in the opposite direction compared to $n = 3$. For normal XY-sequences such a shift cannot induce a resonance shift, as only one modulation function does not allow for a direction.
The major advantage of inducing such a resonance shift is that it allows to delete noise terms in the effective evolution. Assuming an effective Hamiltonian

$$H_{\text{eff}} = \omega_I I_z + A_x S_{\text{eff}} I_x \tag{36}$$

where

$$S_{\text{eff}} = f_1(t)\,(S_x + \epsilon_1 S_y + \epsilon_2 S_z) + f_2(t)\,(S_y + \epsilon_3 S_x + \epsilon_4 S_z) \tag{37}$$

the errors $\epsilon_{1/3}$ would only slightly inhibit polarisation transfer, but the errors $\epsilon_{2/4}$ have a considerable impact. The shift in τ shifts the frequency of $f_{1/2}$ from the resonance and therefore decouples S_z terms from the effective evolution. Only $S_{x/y}$ terms remain at the original resonance due to the rotation induced by α. Figure S4 shows that for $\Delta T/T \approx 2.5\%$ a considerably better resistance to Rabi and Detuning errors is achieved. The values result from an integration over heatmaps like in figure 2c in the main text (with a larger parameter space). Note that everything described in this section is independent of the nuclear spin bath and therefore the resonance shift is equal for all NV centres in an ensemble.

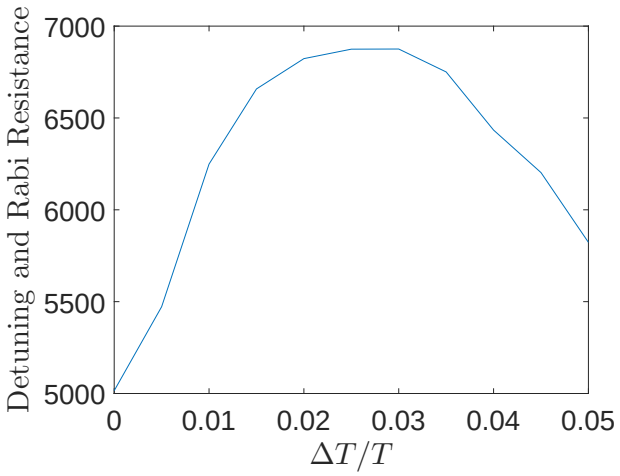

Fig. S4. Error resistance of PulsePol versus the resonance shift. Error resistance (arb. u.) of PulsePol depending on the resonance shift.

Section S7. Hamiltonian with NV centers in nanodiamonds

We apply a strong magnetic field $\gamma_e B \gg D$ along the z direction of laboratory frame of reference for the following technical reasons. (i) The time of the polarization built-up cycle is limited by the NV T_2, and the T_2 of the NV center is prolonged due to better dynamical decoupling at higher magnetic fields. (ii) Large magnetic fields result in longer ^{13}C T_1 relaxation times for polarization built-up. (iii) When $\gamma_e B \gg D$ with γ_e the gyromagnetic ratio, one has a uniform laboratory frame of reference (along the direction of the strong magnetic field) for different orientations of the NV center.
There is however a technical limit on going to very high fields (> 2T) as higher MW power is required, which is more difficult to realize experimentally. PulsePol can still be used at higher magnetic fields even if the MW power is limited by matching the time between the pulses to a higher harmonic of the nuclear Larmor as shown in Eq. (3) in main text, albeit at a tradeoff to the polarization efficiency.
In the strong magnetic field limit, the Hamiltonian can be written as

$$H = DS_{\tilde{z}}^2 + \omega_S S_z + \omega_I I_z + \vec{S}\mathcal{A}\vec{I} + 2\Omega_3(t) S_x \cos(\omega_{MW} t + \varphi) \tag{38}$$

in which the zero-field splitting term is based on the NV orientation $\tilde{z}$, which transforms as

$$S_{\tilde{z}} = S_z \cos\theta + S_x \sin\theta \cos\phi + S_y \sin\theta \sin\phi \tag{39}$$

Here θ is the polar angle between the magnetic field and NV orientation, and ϕ is the azimuthal angle. Going to the rotating frame with respect to $\omega_{MW} S_z$, we have

$$H = D\left(\cos^2\theta S_z^2 + \sin^2\theta S_x^2\right) + (\omega_S - \omega_{MW}) S_z + \omega_I I_z + S_z \vec{\mathcal{A}}\vec{I} + \Omega_3(t)(S_x \cos\varphi + S_y \sin\varphi) \tag{40}$$

The MW pulses are applied to drive the transition of two levels near resonantly (i.e., $m_s = 0$ and $ms = -1$), and the third level is not affected due to large frequency difference. Therefore, the NV centers in nanodiamonds can be simplified to two-level systems, and the Hamiltonian of NV centers interacting with nuclear spins can be simplified to be Eq. (3) with $\Delta = \omega_S - \omega_{MW} + D(\theta)$ in which

$$D(\theta) = D\left(\cos^2\theta + \frac{1}{2}\sin^2\theta - \sin^2\theta\right) = D\left(1 - \frac{3}{2}\sin^2\theta\right) = \frac{D}{4}\left(1 + 3\cos(2\theta)\right) \tag{41}$$

and the MW Rabi frequency is $\Omega(t) = 1/\sqrt{2}\Omega_3(t)$.

Section S8. Depolarization behavior

The numerical results that are compared with experimental data in figure 3 in the main text were obtained by smoothing the actual data that were oscillating fast due to resonances of the free evolution detuning term. Figure S5 also shows the unsmoothed data. For macroscopic polarisation buildup in all applications of interest not only the transfer efficiency is relevant, but also that the transfer is not reversed for other detuning values. Thanks to the implementation of phase errors (see section S6) PulsePol does not destroy a significant amount of polarisation for any detuning when applied in the other direction, i.e. to further polarise an already polarised bath. This is confirmed by the blue data in figure S5 with theoretical simulations and experimentally with PROPI by reversing the polarisation direction.

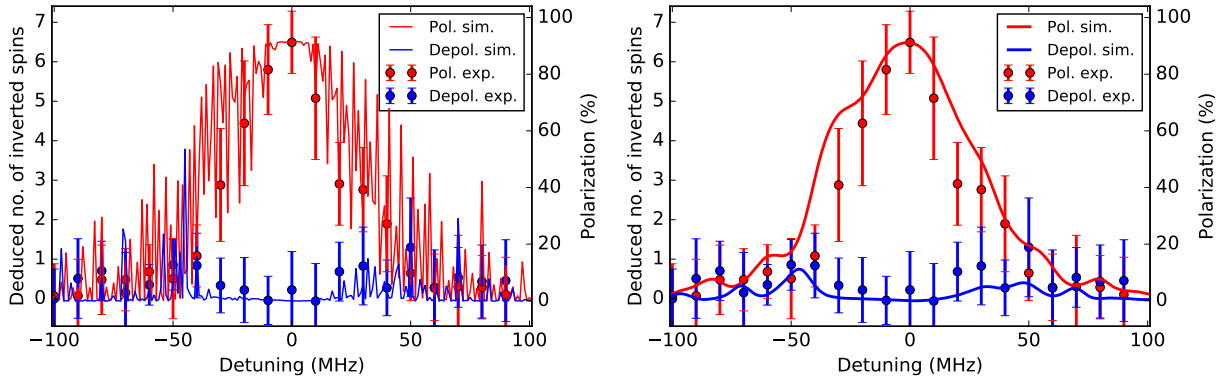

Fig. S5. Comparison between simulation results and experimental data of polarization buildup and depolarization. Simulation results (left: raw data, right: smoothed) compared to the experimental data for polarisation buildup (red) and depolarization (blue).

Section S9. Simulation parameters for shallow NV centers

Here we provide details about the numerical simulations performed to obtain the results of (Fig. 4c) of the main text. 1200 most strongly coupled spins are included in the simulations as these spins account for two thirds of the total coupling strength between the NVs and the whole spin bath. We simulate 100 independent baths of nuclear spins interacting with shallow NV centers that are placed 3 nm below the surface of a bulk diamond. The nuclear spins are assumed to be uniformly and randomly oriented in space. The position of the spins is assumed to be random initially and then a diffusion process is simulated to calculate their positions evolving over time with diffusion coefficients $D = 1.4/2.8 \times 10^{-12}\mathrm{m}^2/\mathrm{s}$ (blue dotted/red dashed curve in Fig. 4c). A magnetic field of strength 0.047 Tesla aligned with the NV crystal axis is applied. The couplings between the NV and the nuclear spins are calculated for different values of time based on their distance from and orientation with respect to the NV center. The NV-center transition frequencies are drawn from a Gaussian distribution with $(2\pi)20$ MHz width. The Rabi frequency is taken as $(2\pi)50$ MHz and the nuclear Larmor frequency is $(2\pi)2$ MHz.

During evolution under PulsePol, the entanglement between the different constituents is limited so the state of the NV and the spins can be efficiently represented by a matrix product state (MPS). The time evolution is simulated using the time-evolution via block decimation (TEBD) algorithm on the MPS representation. Owing to the robustness to protocol to the frequency fluctuation, the NV centers effect a high degree of nuclear polarization in the spin bath as depicted in (Fig. 4c).